Effects of particle size and spacing on the optical properties of gold nanocrystals in alumina

Juan Wang, W. M. Lau, and Quan Li[a)]
Department of Physics, The Chinese University of Hong Kong, Shatin, New Territory, Hong Kong

(Received 13 October 2004; accepted 11 January 2005; published online 24 May 2005)

Au-particle/Al_2O_3-matrix nanocomposite thin films with a narrow Au particle size distribution were fabricated by radio-frequency magnetron cosputtering. The films were characterized both chemically and structurally using x-ray photoelectron spectroscopy, x-ray diffraction, and transmission electron microscopy. The optical absorption of samples with various Au particle sizes and concentrations were measured using an ultraviolet/visible-spectrometer. Both the Au nanoparticle size and the Au concentration increase result in a redshift of the Au surface-plasmon resonance energy. The redshift due to the size effect is concluded as mainly originating from the size-dependent dielectric function of Au core electrons and a semiquantitative description of its size dependence is presented. The experimental result describing the concentration effect suggests a deviation from the conventional Maxwell-Garnett effective medium theory, which can be corrected by introducing the multipole effect based on the dipole-dipole interaction model. © *2005 American Institute of Physics*. [DOI: 10.1063/1.1868052]

I. INTRODUCTION

In recent years, noble-metal-particle/matrix nanocomposite materials have aroused great interest in both basic scientific research and technical applications such as nonlinear optical devices and optical waveguides.[1–4] The optical absorption of the noble-metal particles is dominated by the resonant coupling of the incident field with the collective oscillations of conduction electron(s) [the so-called surface-plasmon resonance (SPR)].[5,6] The specific absorption is determined by both the conduction electrons in the metal particle and the coupling field in the vicinity of the individual particle. Different from the alkali metals, the collective oscillations of conduction electron(s) of the noble-metal particle are greatly affected by the core electrons (especially *d* band electrons).[7,8] In general, theoretical models describing the surface-plasmon resonance of noble-metal particles (in a medium) have been well developed. Among them, Mie theory is successful in explaining the coupling of isolated spherical particles with the external field in the quasistatic regime, but it breaks down as a result of the interactions between the particles when the interparticle distance is small.[7,9–11] The Maxwell-Garnett (MG) effective medium theory agrees better with the experimental results by introducing the particle-particle interactions, as well as the modifications induced by the matrix material and the nonspherical particle shape.[12]

As a comparison to the theoretical works, the experimental data in the literature are much scattered and in many cases confusing. Although it has been identified that the SPR is influenced by four factors (including the metal particle size, as well as the concentration, shape, and dielectric function of the surrounding materials),[6,7,10] the complicated sources of the first two factors make it difficult to differentiate them experimentally. Moreover, the lack of experimental data in the small size regime causes more confusion when compared with various theoretical models. In addition, there is always a problem with the credibility of experimental data, i.e., a large particle size distribution (resulting from the fabrication techniques) leads to an averaged response. In order to address the above issues, a systematic study on the nanocomposite films, especially in the small size range with narrow size distribution, is desired.

In the present work, Au-particle/Al_2O_3-matrix composite films with narrow particle size distributions and various gold concentrations were deposited using radio-frequency (rf) magnetron sputtering. The SPR results from the Au nanoparticles in the composite films were studied as functions of both the Au particle size and concentration. The experimental data were then fitted and compared to various theoretical models in order to determine the size and concentration effects. Finally, the discrepancies between the experimental results and the existing theoretical models are discussed.

II. EXPERIMENTAL

The Au/Al_2O_3 nanocomposite thin films were deposited by rf magnetron cosputtering in a high vacuum chamber with a base pressure of 5×10^{-6} Torr. The two targets were Au (99.99%, Goodfellow) and Al_2O_3 (99.99%, Goodfellow) plates. Different types of substrates were used for different characterizations, i.e., Si wafers for the microstructure characterization and quartz glass sheets for the optical absorption measurement. In order to obtain the desired metal particle size and concentration, deposition parameters, including the two target powers, deposition pressure, and the annealing temperature, were independently varied. Selected samples with different volume concentrations were further annealed from 200 °C to 900 °C in an Ar environment for 2 h. The details are listed in Table I.

[a)]Author to whom correspondence should be sent. Electronic mail: liquan@phy.cuhk.edu.hk

TABLE I. Detailed deposition parameters, the resulting metal concentrations, filling factors, and particle sizes (radius) in different series of samples.

	Sample number	Au target power (w)	Al_2O_3 target power (w)	Ar pressure (mTorr)	Au atomic concentration (at. %)	Au filling factor	Particle radius (nm)	Annealing temperature (°C)
Size effect (anneal -ing) series	A1	20	400	10	1.41	0.0276	1.1	as-prepared
							1.4	300
							1.6	400
							1.7	500
							2.1	600
	A2	20	350	30	12.16	0.2155	1.7	as-prepared
							1.9	200
							2.1	300
							2.9	500
							3.2	600
							8.7	900
Concen -tration effect series	C	20	400	10	1.41	0.0276	1.1	
		20	350	1	2.52	0.0488	1.3	
		20	300	1	4.15	0.0791	1.4	
		30	350	10	6.57	0.1225	1.4	
		20	190	1	9.94	0.1797	2.5	
		30	400	1	11.09	0.1984	2.0	
		20	350	30	12.16	0.2155	1.8	
		30	350	1	13.95	0.2434	2.8	
		20	235	10	14.30	0.2488	1.8	
		40	350	1	15.84	0.2719	3.1	
		30	300	1	16.09	0.2756	2.8	
		30	235	1	16.96	0.2884	2.9	
		30	190	1	17.68	0.2988	3.0	
		30	300	10	18.31	0.3079	2.1	
		40	300	10	22.00	0.3589	2.2	
		30	400	50	23.44	0.3779	3.0	
		30	300	50	30.07	0.4596	2.7	
		30	350	30	30.81	0.4691	2.5	
		30	235	10	32.78	0.4918	2.6	

The samples were then characterized both chemically and structurally using different techniques. First, the atomic concentration of the Au was examined by an x-ray photoelectron spectroscopy (XPS) in-depth profile, so that information on both the film surface and the film interior can be obtained. The atomic concentration was then converted to the volume concentration (also known as the filling factor) by a simple calculation.[13] The general crystallinity of the film was investigated by glancing angle x-ray diffraction (XRD), and the mean particle size (refers to the radius R of the spherical particles) can be obtained based on the Scherrer formula.[14] In order to find the metal particle size distribution and the detailed microstructure of the thin film, transmission electron microscopy [(TEM), Philips CM 120 and Tecnai 20 ST] was employed. Finally the optical absorption of the composite films were studied using an UV/VIS spectrometer operating in the wavelength range of 350–800 nm.

III. THE OPTICAL RESPONSE OF THE NANOCOMPOSITE THIN FILMS—MAXWELL-GARNETT EFFECTIVE MEDIUM THEORY

Among all the existing theories, the MG effective medium theory is the most comprehensive one. It includes the contributions from the dielectric properties of both the particles and the matrix, the shape of the individual particles, and the particle-particle interactions. Under the mean field approximation, the optical property of the nanocomposite system is described by ε_{eff} as a whole, which is the dielectric function of the effective medium, as defined in the generalized Maxwell–Garnett (MG) effective medium theory:[15,16]

$$\frac{\varepsilon_{\text{eff}} - \varepsilon_m}{L\varepsilon_{\text{eff}} + (1-L)\varepsilon_m} = f\frac{\varepsilon_1(\omega) - \varepsilon_m}{L\varepsilon_1(\omega) + (1-L)\varepsilon_m}, \tag{1}$$

where $\varepsilon_1(\omega)$ is the real part of the dielectric function of the metal particle, ε_m the dielectric function of the surrounding medium, L the shape factor (or depolarization factor) of the particle,[17] and f the filling factor (also known as volume concentration, which reflects the extent of the particle-particle interactions by means of their dipolar fields). In the present study, the shape factor L is taken as $1/3$ for spherical particles[6] (this is justified in later sections), which leads to a simplification of Eq. (1) (Ref. 18) to

$$\frac{\varepsilon_{\text{eff}} - \varepsilon_m}{\varepsilon_{\text{eff}} + 2\varepsilon_m} = f\frac{\varepsilon_1(\omega) - \varepsilon_m}{\varepsilon_1(\omega) + 2\varepsilon_m}. \tag{2}$$

The real part of the metal particle dielectric function $\varepsilon_1(\omega)$ represents the optical properties of a single particle and can be expressed as[6,7,19]

$$\varepsilon_1(\omega) = \varepsilon_d' - \frac{\omega_p^2}{\omega^2 + 1/\tau^{*2}}. \quad (3)$$

The term ε_d' refers to the real part of the dielectric function contributed by the core electrons (especially the *d* electrons). The second term is the contribution from the conduction electrons based on the Drude free electron model. ω_p is the bulk plasmon frequency conventionally defined as $\omega_p = (ne^2/\varepsilon_0 m_{\text{eff}})^{1/2}$.[20] τ^* is the electron relaxation time, which can be neglected in the case of free electron metals, as $\tau^* \ll \omega_p$,[21] leading to a simplified version of Eq. (3):

$$\varepsilon_1(\omega) = \varepsilon_d' - \frac{\omega_p^2}{\omega^2}. \quad (4)$$

Based on the MG theory, the surface-plasmon resonance occurs when

$$\varepsilon_1(\omega_s)(1-f) + \varepsilon_m(2+f) = 0, \quad (5)$$

where ω_s is the surface-plasmon resonance frequency.[10,18,22]

On the condition where the Mie theory holds for the ideally isolated particle system ($f \approx 0$), Eq. (5) is simplified to

$$\varepsilon_1(\omega_s) = -2\varepsilon_m, \quad (6)$$

which further gives the Mie resonance ω_s (Ref. 23) as

$$\omega_s = \frac{\omega_p}{\sqrt{2\varepsilon_m + \varepsilon_d'(\omega_s)}}. \quad (7)$$

In more general cases where $f > 0$:

$$\omega_s = \frac{\omega_p}{\sqrt{\frac{2+f}{1-f}\varepsilon_m + \varepsilon_d'(\omega_s)}}. \quad (8)$$

The medium dielectric function ε_m is taken as a constant number of 3.1 for the Al_2O_3 matrix in the energy range examined.[7,24] Therefore the above equation suggests that three factors will affect the surface-plasmon frequency:

(1) ω_p, which relates to the conduction electron density.
(2) $\varepsilon_d'(\omega_s)$, the core electrons contribution to the dielectric constant in the vicinity of the surface-plasmon resonance.
(3) f, the volume concentration of the metal.

IV. RESULTS AND DISCUSSIONS

A. General description of the as-prepared thin films

The XPS in-depth profiles indicate that the chemical compositions of the film interiors remain unchanged. In general, the Au concentrations in the as-prepared films increase with increasing Au target power, decreasing Al_2O_3 target power, and increasing Ar pressure. The same dependence of the particle size on the two target powers is found. Nevertheless, the trend that the particle size decreases with increasing Ar pressure only holds at low Au concentrations. These trends can be found in Table I, which also summarizes the structural characteristics of the annealed films. The thicknesses of all the films are in the range of 100–200 nm, which allows sufficient light transmission in the optical absorption measurement. The transmission colors of the films change from brownish to red and purple owing to the changing of the SPR frequency as well as the background (interband transitions) in the absorption spectrum.

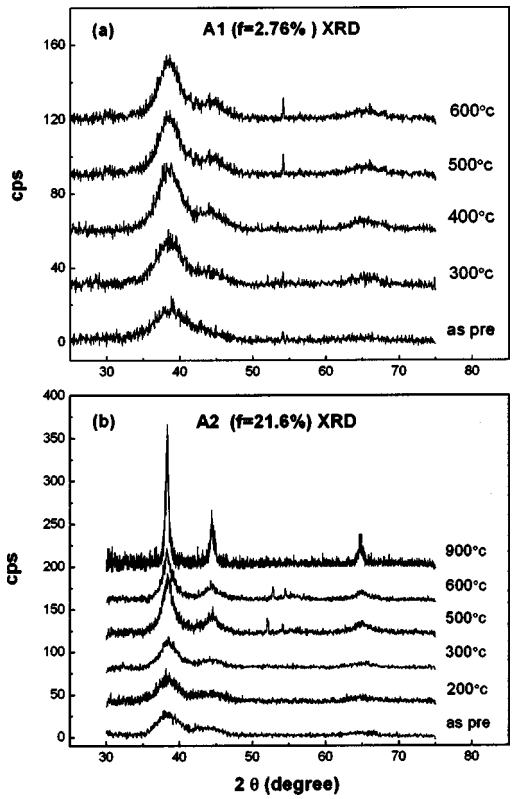

FIG. 1. XRD results of the two annealing series: (a) A1 (f=2.76%), (b) A2 (f=21.6%).

B. Size effect on SPR shift

XPS results show that the Au volume concentrations of samples A1 and A2 are 2.76% and 21.6%, respectively. Such concentrations remain unchanged after the annealing process. No peak shape change or any chemical shift is detected for all the annealed samples, compared to those of the as-deposited ones. We therefore conclude that the Au remains in its metallic form in all of the samples. The general crystallinity of the annealed series A1 is disclosed by the XRD results shown in Fig. 1(a). Based on the Scherrer equation, the average size (radius) of the Au particles before and after annealing are estimated to range from ~1.1 nm (as-prepared) to ~2.1 nm (600 °C) as listed in Table I. The particle size evolution of the annealed series A1 is further confirmed by TEM investigations [Fig. 2(a)], which also reveal the spherical particle shape and the narrow size distribution (standard deviation of the radius is 0.23 nm) of the Au particles in individual samples. A similar trend is observed in the annealed series A2, in which the Au particle radius increases from ~1.7 nm to ~8.7 nm [estimated from the XRD results in Fig. 1(b) as the annealing temperature is raised to 900 °C]. It should be pointed out that the concentration and the separation distance of the Au particles cannot be measured directly from the TEM micrograph, which is

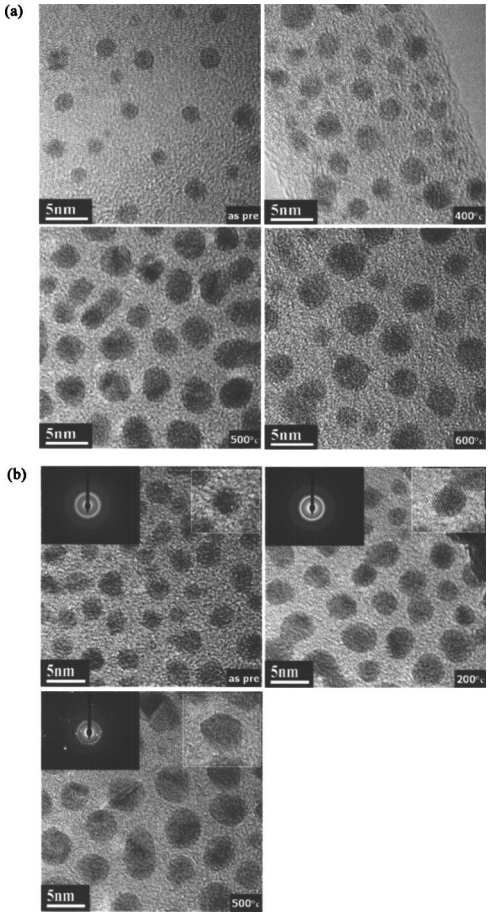

FIG. 2. (a) TEM images of several selected samples from the annealing series A1, showing the evolution of the particle size as temperature increases. (b) High-resolution TEM images and the corresponding selected area diffraction patterns of several selected samples from the annealing series A2.

effectively the two-dimensional projection of the sample due to its finite thickness. In addition, the transmission electron diffraction and high-resolution TEM are performed on these samples in order to determine the microstructure of the Au particles. Representative results of several selected films from series A2 are shown in Fig. 2(b) as examples. The selected area electron diffraction patterns change from diffused rings to sharp rings and then to well-defined diffraction spots as the particle sizes increase from $R=1.7$ nm (as-prepared) to 1.9 nm (200 °C), and then to 2.8 nm (500 °C), respectively. The lattice spacing of the Au particles with different size is estimated using both transmission electron diffraction (TED) and high-resolution TEM (HREM), while no difference is detected for all the samples examined within the experimental error.

The corresponding optical absorption spectra of series A1 and A2 are shown in Fig. 3. The SPR peaks of both series are located in the wavelength range from ~520 nm to ~565 nm. A redshift in the SPR is detected in both series for samples annealed to higher temperatures. The surface-plasmon resonance energy is then plotted as a function of the reciprocal of the Au particle radius for both series (Fig. 4). Curve fitting shows that both of them deviate from linear relations. In addition, an obvious "jump" exists in-between the two annealing series, as marked by the arrow in Fig. 4.

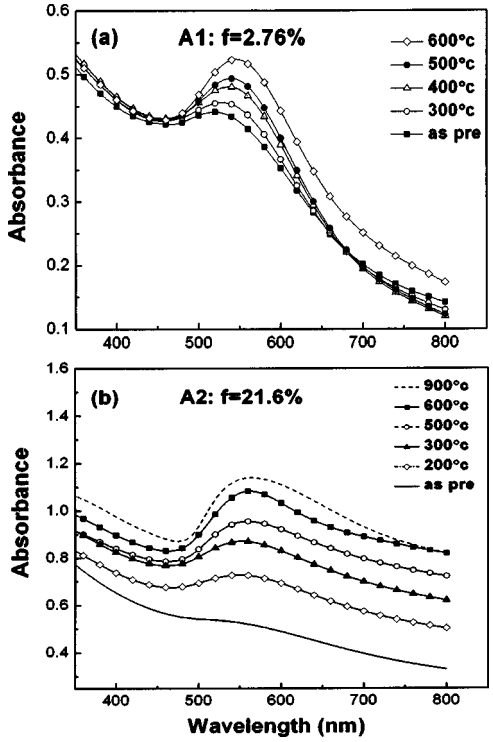

FIG. 3. Optical absorption spectra of the annealing series (a) A1 and (b) A2.

The observed SPR redshift with increasing Au particle size is generally ascribed to the so-called "size effect," which includes both the extrinsic size effect and the intrinsic size effect. The extrinsic size effect refers to the size-dependent interference of the retarded electromagnetic wave (the phase retardation induced higher multipoles), which is only considered when the particle size is comparable to the wavelength of the incident light. Such effects can be ignored when the particle diameter is less than 20 nm,[7] which satisfies the present experimental results.

The intrinsic size effect of the particle material is restricted to the quasistatic regime ($R \leqslant \lambda$), and is expressed in the form of a size-dependent dielectric function, i.e., $\varepsilon(\omega, R)$. The phenomenological dielectric function $\varepsilon(\omega, R)$, obtained either from experiments or theoretical calculations, indicates the averaged contributions from all electronic and structural factors of the particles. In order to find the origin of the SPR shift with the particle size as stated above, we studied the

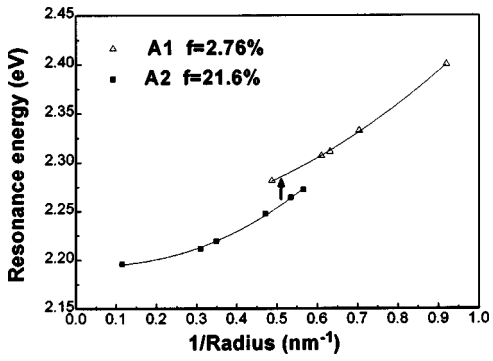

FIG. 4. The surface-plasmon resonance energy as a function of the reciprocal of the Au particle size in sample series A1 and A2.

intrinsic size effect on the two parameters based on the expression of the real part of the metal particle dielectric function $\varepsilon_1(\omega,R)$ in Eq. (4) [which further determines the SPR frequency in Eq. (7)], i.e., the size dependence of $\omega_p(R)$ and $\varepsilon_d'(\omega)$.

We discuss the size effect on $\omega_p(R)$ first. Knowing from the definition of $\omega_p(R)$, $\omega_p=(ne^2/\varepsilon_0 m_{\text{eff}})^{1/2}$, it is mainly determined by the electron density n. Regarding this aspect, the "spill out" effect in very small particles[7,25] and the lattice contraction effect[26] have been well established in the literature in explaining the changes in $\omega_p(R)$ as the metal particle size varies. In the first case, the "spill out" of the free electrons on the particle surface leads to a decreased volume-averaged electron density n, and finally a redshift of the SPR energy due to the decrease in $\omega_p(R)$. This effect, which is essential in interpreting the redshift of the SPR with decreasing particle size in alkali metals, is, however, trivial in the case of Au due to the strong screening of its d electrons [a large $\varepsilon_d'(\omega)$ value].[23] In the latter case of $\omega_p(R)$, one of the direct consequences of the lattice constant variation is the change of the electron density n. Such lattice contraction, resulting from the surface stress (or the interface stress for embedded particle) of the particles,[27] can be described as

$$\frac{\Delta a}{a_0}=-\frac{2}{3}\frac{KS}{R}, \tag{9}$$

where a_0 is the lattice constant and Δa the lattice contraction value. For metals with face-centered-cubic structure the expression of $\omega_p(R)$ can be written as

$$\omega_p(R)=(4e^2/a^3\varepsilon_0 m_{\text{eff}})^{1/2}=\omega_p(\infty)\frac{a_0^{3/2}}{a^{3/2}}$$

$$=\omega_p(\infty)\left(1-\frac{3}{2}\frac{\Delta a}{a_0}\right),$$

and thus

$$\omega_s=\frac{\omega_p(\infty)\left(1+\dfrac{KS}{R}\right)}{\sqrt{\dfrac{2+f}{1-f}\varepsilon_m+\varepsilon_d'(\omega_s)}}, \tag{10}$$

which indicates a linear dependence of the ω_s on $1/R$.

Nevertheless, both HREM and TED results of the Au nanoparticles in series A1 and A2 reveal that the lattice contraction, if any, is too small to be distinguished. Moreover, both curves in Fig. 4 deviate from linear function, indicating that such lattice concentration effects, although possibly important in affecting the SPR shift in some specific cases,[26] is not a major factor in the current study.

We can now focus on the contribution from $\varepsilon_d'(\omega)$ after eliminating that from $\omega_p(R)$. It is known that the core electrons have important influences on the SPR energy of the noble-metal particles when considering the screening effect from the d electrons.[7,28–30] As the "spill out" of the free electrons on the particle surface, they are incompletely embedded inside the ionic-core background, leading to the ineffective screening at the skin region. As a consequence, the dielectric property (characterized by ε_d') of the skin region is different from that of the inner part. Regarding this, a two-region (or multilayer) dielectric model is employed to interpret the size dependence of the total ε_d'. The bulk value of Au ε_d' in the vicinity of ω_s is $\sim$10 and $\varepsilon_d'(R-a<r<R)\approx 1$ in the surface skin region.[23,31] Therefore, ε_d' can be treated as an effective core polarization with both bulk and surface terms. The decreasing value of ε_d' (as the particle size decreases) originates from the increasing contribution from the polarization-free surface, as the surface-to-volume ratio increases. A more explicit understanding can be obtained from the time-dependent local-density-approximation (TDLDA) calculations, taking into account the d electrons and the matrix screen effects.[32]

However, the ineffective screening on the surface layer is not the only factor that contributes to the change of ε_d', especially in the case of Au. In fact, the much stronger blueshift trend observed in gold particles is a consequence of the ω dependence of $\varepsilon_d'(\omega)$.[8,31,33] In gold, the edge of the interband transition (the onset of a weak transition at 1.94 eV near X, and a stronger one at 2.45 eV near L in the Brillouin zone) coincides with the position of the SPR at $\sim$2.2 eV.[6,34] The influence of the size-dependent interband transition on the SPR must be taken into consideration. The interband transition is mainly determined by the material electronic structures, which can be influenced by the following particle-size-related factors: (1) the lattice-contraction-induced variation of the lattice constant;[35,36] (2) the lattice defects (impurities, point defects, multidomain structures with grain boundaries), etc.,[7] (3) special surface/interface states due to the structural reconstruction of the surface or the particle immersion in the alumina matrix,[37–40] and (4) the charge transfer between the particle and the matrix at the particle/matrix interface.[41,42] All these affect the electronic structure of the Au particles, and thus contribute to $\varepsilon_d'(\omega)$.

Therefore, in addition to the expectations from the TDLDA calculations, the influence of the interband transition must be considered. It is important to find out how the core electron dielectric function $\varepsilon_d'(\omega)$ would change with the particle size. In this work, the size dependence of $\varepsilon_d'(\omega_s)$ is obtained from Eq. (8) by measuring ω_s as a function of size, taking $\omega_p(\infty)=9.1$ eV/$\hbar$ (the bulk plasmon resonance frequency for Au), $\varepsilon_m=3.1$ for the Al_2O_3 matrix, and $f=2.76\%$ and 21.6% for A1 and A2, respectively. Both series in Fig. 5 demonstrate the general trend of $\varepsilon_d'(\omega_s)$, decreasing as the particle size decreases and with a larger decreasing rate in the small size region (the radius is less than 5 nm). Intuitively, $\varepsilon_d'(\omega_s)$ should be independent of the metal concentration; however, the two series with different concentration (presented in Fig. 5) do not join and cannot be fitted with a single curve. In fact, a similar "jump" is already observed in Fig. 4. The jump there originates from the Au concentration difference of the two series. The Au concentration of series A1 is close to the low concentration limit of the ideally isolated particles so that the influence of the interparticle interactions can be ignored and it can be well modeled by the MG theory or even the Mie theory [$f\approx 0$ and $\varepsilon_1(\omega_s)=-2\varepsilon_m$], while series A2 belongs to the interacting system because of the much higher Au concentration (>20%). A redshift in the SPR energy is detected in Fig. 4 when the

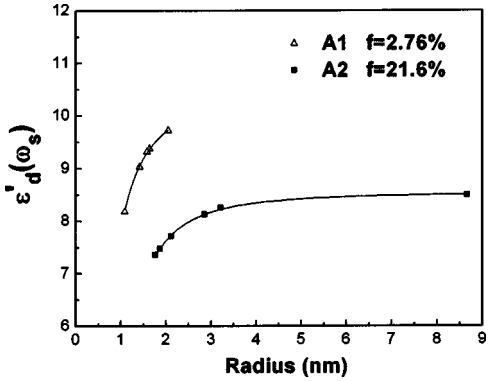

FIG. 5. Calculated $\varepsilon'_d(\omega_s)$ values as a function of the Au particle size in the sample series A1 and A2.

particle concentration becomes larger, which leads to the investigation of the concentration effect as discussed in the next section.

C. Concentration effect

In this series of experiments, we change the Au volume concentration in the samples at several specific particle sizes. Detailed information can be found in Table I. The surface-plasmon resonance energies of these samples were measured and plotted as a function of the volume concentration f in Fig. 6. A theoretical curve describing the SPR energy as a function of the Au concentration is also plotted in the same figure (those with open circles) based on the MG theory using the bulk value of $\varepsilon'_d(\omega_s)$. In general, the experimental SPR energies redshift with the increasing f, which is similar to that of the MG curve. Nevertheless, they do deviate from the theoretical one and the data points are much more scattered.

The redshift of the SPR with increasing f can be explained by the interactions among the individual particles.[12,43–45] It is conventionally modeled by the MG effective medium theory, which also qualitatively explained the red "jump" in Fig. 4. The scatter of the experimental data points may partially result from the different particle size [as explained by the intrinsic size effect, which has been demonstrated in Fig. 5 in the form of the size dependent $\varepsilon'_d(\omega_s, R)$].

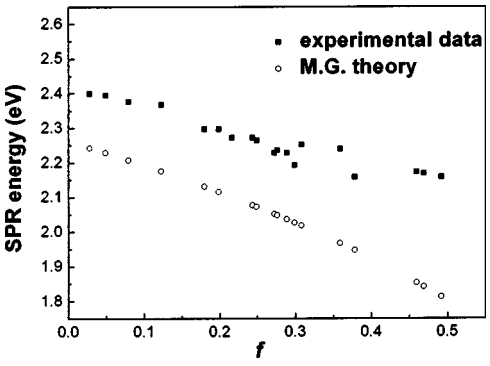

FIG. 6. Theoretical (open circles) and experimental (solid squares) SPR energy as a function of the Au volume concentration in the concentration series. The experimental curve consists of data points from different particle sizes.

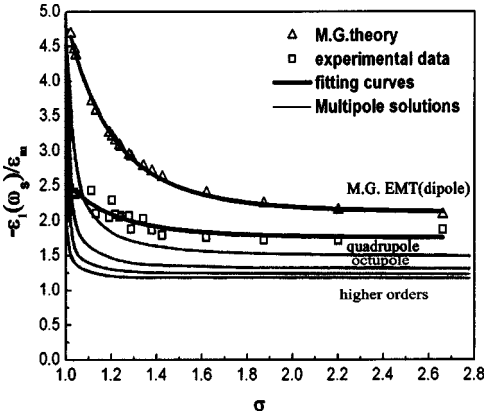

FIG. 7. The plot of experimental $-\varepsilon_1(\omega_s)/\varepsilon_m$ values as a function of the particle separation σ (open squares). The theoretical curve is plotted using the MG theory (open triangles) and multipole treatment according to Ref. 47 (thin lines).

We can now address the deviations of the experimental data from the theoretical results in Fig. 6. Such deviations suggest a discrepancy between the experimental results and the conventional MG theory, which inspires us to look for other possible models.

Another theory to describe the absorption properties of a highly concentrated particle system is the dipole-dipole interaction model. It is known that a single particle with a dielectric constant ε_1 in a uniform field can be treated as a dipole having a moment proportional to $(\varepsilon_1+2\varepsilon_m)^{-1}$. The surface resonance absorption occurs when $\varepsilon_1(\omega_s)/\varepsilon_m=-2$, which is the Mie condition and valid only in the case of very dilute particle systems.[9,10] The dipole-dipole interaction model takes other nearby "dipoles" into consideration, which contributes to the nonuniform field at the position of the dipole of interest so that higher order multipoles are excited.[46] The effective field then results from all the nearby multipoles. The total effect introduced by the dipole-dipole interaction (multipole excitation) is proportional to $(R/d)^{2l+1}$, where d is the distance between the neighboring particles, and l is the multipole order ($l=1$ for dipole, $l=2$ for quadrupole, etc.).[47,48]

The MG effective medium theory using the mean field approximation assumes that the field outside a particle is a superposition of the external field and all the dipole fields of the neighboring particles,[10] which is comparable to the first-order approximation of the dipole-dipole interaction model.[11] When higher-order multipole terms are considered, the resonance condition is expected to be different, as suggested by Claro in Ref. 47. In his work, the resonance condition, i.e., the value of the $-\varepsilon_1(\omega_s)/\varepsilon_m$, is calculated as a function of the interparticle separation σ ($\sigma=d/2R$) and the multiplicity of their solutions results from the resonance excitation of multipoles of all orders.

Then the $-\varepsilon_1(\omega_s)/\varepsilon_m$ value calculated from our experimental results is plotted as a function of the particle separation σ in Fig. 7, where the theoretical curve based on the MG theory (dipole solution) and higher-order multipole solutions are also plotted as a reference. σ is calculated from the Au volume concentration assuming that the film is a uniform composite with spherical particles of radius R and interpar-

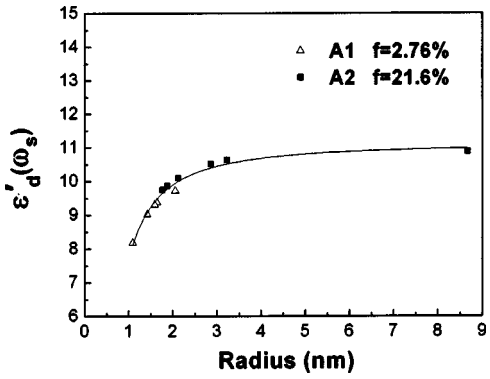

FIG. 8. The modified $\varepsilon_d'(\omega_s)$ as a function of the Au particle size using the experimental $-\varepsilon_1(\omega_s)/\varepsilon_m$ values from Fig. 7 (with the multipole approximation).

ticle distance d, i.e., $f=V_{\mathrm{Au}}/V_{\mathrm{total}}=\frac{4}{3}\pi R^3/d^3$, and $-\varepsilon_1(\omega_s)/\varepsilon_m$ from the equation $\varepsilon_1(\omega_s)=\varepsilon_d'-(\omega_p^2/\omega_s^2)$, where $\omega_p(\infty)=9.1$ eV/$\hbar$ and $\varepsilon_d'(\omega_s)$ is estimated from the data in Fig. 5, using the curve with lower Au concentration (as it is close to the low concentration limit and can be treated as the ideally isolated particles system, where the Mie theory holds).

Fig. 7 shows that the value of $-\varepsilon_1(\omega_s)/\varepsilon_m$ calculated from the experimental result increases as the interparticle separation σ decreases, which is consistent with the trend of the MG curve. However, the experimental data sit below the MG curve (dipole solution) and the deviation in the region of the smaller interparticle separation is generally larger than that in the larger separation region, which indicates the inaccuracy of the dipole solution and the necessity of higher-order multipole solutions. Nevertheless, the experimental data cannot be exactly fitted by any single solution with a specific multipole order. This indicates that the excitations of multipoles with different orders contribute together to the experimental observations, and multipole(s) with specific order may be dominant in different interparticle separation regions.

Our experimental results agree better with the multipolar treatment of the dipole-dipole interaction model than the conventional MG theory, especially when the Au volume concentration gets larger. We therefore replot the curves in Fig. 5 using the experimental $-\varepsilon_1(\omega_s)/\varepsilon_m$ value (from Fig. 7) instead of the $(2+f)/(1-f)$. This leads to the disappearance of the original jump in-between the two series as shown in Fig. 8, indicating the correction to the error induced by the dipole assumption. In fact, the multipole treatment hardly affects the result of series A1, but significantly modifies that of A2. This is consistent with the experimental condition that A1 is a very dilute system with very weak particle-particle interactions, while the interaction effect can no longer be ignored in a series of A2 with a much higher Au concentration. Finally the joined two series can be fitted by a single curve, which reveals the corrected size dependence on $\varepsilon_d'(\omega_s)$ of Au particles.

V. CONCLUSIONS

Au-nanoparticles/Al_2O_3-matrix nanocomposite thin films with various Au particle sizes and concentrations were deposited by rf–magnetron sputtering. At controlled experimental conditions, the sizes of the Au particles in the as-prepared films are relatively small (particle radius from 1.1 to 3.1 nm) and have a narrow size distribution. A redshift of the surface-plasmon resonance was observed when increasing either the Au particle size (size effect) or the Au concentration (concentration effect). The size effect mainly originates from the size-dependent dielectric function of the Au core electrons, while the size influences on ω_p can be almost neglected. The dependence of the core electron dielectric function on the Au particle size results from both the ineffective screening at the surface region and the changing of the electronic structures at the interband transitions. A semiquantitative description of the size dependent $\varepsilon_d'(\omega_s)$ was given based on the experimental data. In the study of the concentration effect, a discrepancy between the experimental result and the conventional MG EM theory was identified, and the dipole-dipole interaction model considering the multipole effect appears to be a better solution, especially in the high Au concentration regime.

ACKNOWLEDGMENTS

The authors acknowledge the technical assistance from A. S. K. Li. This work was funded by the Hong Kong Innovation Technology Fund under reference No. ITS/070/03 and ITS/122/01, the RGC fund (project No. CUHK 4182/04E), and RGC direct allocation in the Chinese University of Hong Kong under project No. 2060261.

[1] C. Flytzanis, F. Hache, M. C. Klein, D. Ricard, and Ph. Roussignol, in *Progress in Optics XXIX*, edited by E. Wolf (Elsevier, New York, 1991).
[2] N. Pinçon, B. Palpant, D. Prot, E. Charron, and S. Debrus, Eur. Phys. J. D **19**, 395 (2002).
[3] S. A. Maier, M. L. Brongersma, P. G. Kik, S. Meltzer, A. A. G. Requicha, and H. A. Atwater, Adv. Mater. **13**, 1501 (2001).
[4] H. Ditlbacher, J. R. Krenn, B. Lamprecht, A. Leitner, and F. R. Aussenengg, Opt. Lett. **25**, 563 (2000).
[5] U. Kreibig and P. Zacharias, Z. Phys. **231**, 128 (1970).
[6] D. Dalacu and L. Martinu, J. Appl. Phys. **87**, 228 (2000).
[7] U. Kreibig and M. Vollmer, *Optical Properties of Metal Clusters* (Springer, New York, 1995).
[8] J. Lermé, B. Palpant, B. Prével, M. Pellarin, M. Treilleux, J. L. Vialle, A. Perez, and M. Broyer, Phys. Rev. Lett. **80**, 5105 (1998).
[9] G. Mie, Ann. Phys. **25**, 377 (1908).
[10] L. Genzel and T. P. Martin, Surf. Sci. **34**, 33 (1973).
[11] Z. X. Liu, H. H. Wang, H. Li, and X. M.Wang, Appl. Phys. Lett. **72**, 1823 (1998).
[12] J. C. Maxwell-Garnett, Philos. Trans. R. Soc. London **203**, 385 (1904); **205**, 237 (1906).
[13] $$f = V_{\mathrm{Au}}/V_{\mathrm{total}} = \frac{\dfrac{\text{at.\%} \times \text{molecular mass}}{\text{density}} \text{ of Au}}{\dfrac{\text{at.\%} \times \text{molecular mass}}{\text{density}} \text{ of Au} + \dfrac{\text{at.\%} \times \text{molecular mass}}{\text{density}} \text{ of } Al_2O_3}.$$
[14] B. E. Warren, *X-ray Diffraction* (Dover, New York, 1990).
[15] R. W. Cohen, G. D. Cody, M. D. Coutts, and B. Abeles, Phys. Rev. B **8**, 3689 (1973).
[16] P. Chylek and V. Srivastava, Phys. Rev. B **27**, 5098 (1983).
[17] D. E. Aspnes, Phys. Rev. Lett. **48**, 1629 (1982).
[18] S. K. Mandal, R. K. Roy, and A. K. Pal, J. Phys. D **35**, 2198 (2002).
[19] A. Hilger, M. Tenfelde, and U. Kreibig, Appl. Phys. B: Lasers Opt. **73**, 361 (2001).
[20] C. Kittel, *Introduction to Solid State Physics* (Wiley, New York, 1996).

[21]R. Antoine, P. F. Brevet, H. H. Girault, D. Bethell, and D. J. Schiffrin, Chem. Commun. **19**, 1901 (1997).
[22]P. Sheng, Phys. Rev. Lett. **45**, 60 (1980).
[23]B. Palpant, B. Prével, J. Lermé, E. Cottancin, M. Pellarin, M. Treilleux, A. Perez, J. L. Vialle, and M. Broyer, Phys. Rev. B **57**, 1963 (1998).
[24]E. D. Palik, *Handbook of Optical Constants of Solids* (Academic Press, Orlando, 1991).
[25]W. A. de Heer, Rev. Mod. Phys. **65**, 611 (1993), and references therein.
[26]W. Cai, H. Hofmeister, and M. Dubiel, Eur. Phys. J. D **13**, 245 (2001).
[27]C. Solliard and M. Flueli, Surf. Sci. **156**, 487 (1985).
[28]V. V. Kresin, Phys. Rev. B **51**, 1844 (1995).
[29]A. Liebsch, Phys. Rev. B **48**, 11317 (1993).
[30]L. Calmels, J. E. Inglesfield, E. Arola, S. Crampin, and T. Rasing, Phys. Rev. B **64**, 125416 (2001).
[31]B. Prével *et al.*, Nanostruct. Mater. **12**, 307 (1999).
[32]L. Serra and A. Rubio, Z. Phys. D: At., Mol. Clusters **40**, 262 (1997).
[33]H. Ehrenreich and H. R. Philipp, Phys. Rev. **128**, 1622 (1962).
[34]M. Guerrisi, R. Rosei, and P. Winsemius, Phys. Rev. B **12**, 557 (1975).
[35]P. Picozzi, S. Santucci, M. De Crescenzi, F. Antonangeli, and M. Piacentini, Phys. Rev. B **31**, 4023 (1985).
[36]D. Zanchet, H. Tolentino, M. C. M. Alves, O. L. Alves, and D. Ugarte, Chem. Phys. Lett. **323**, 167 (2000).
[37]G. B. Bachelet, F. Bassani, M. Bourg, and A. Julg, J. Phys. C **16**, 4305 (1983).
[38]S. Grabowski, M. E. Garcia, and K. H. Bennemann, Phys. Rev. Lett. **72**, 3969 (1994).
[39]C. Q. Sun, H. L. Bai, S. Li, B. K. Tay, and E. J. Jiang, Acta Mater. **52**, 501 (2004).
[40]W. Krakow, M. Jóse-Yacamán, and J. L. Aragón, Phys. Rev. B **49**, 10591 (1994).
[41]L. Yang, G. H. Li, and L. D. Zhang, Appl. Phys. Lett. **76**, 1537 (2000).
[42]H. Hövel, S. Fritz, A. Hilger, U. Kreibig, and M. Vollmer, Phys. Rev. B **48**, 18178 (1993).
[43]J. P. Kottman and O. J. F. Martin, Opt. Lett. **8**, 655 (2001).
[44]W. Rechberger, A. Hohenau, A. Leitner, J. R. Krenn, B. Lamprecht, and F. R. Aussenegg, Opt. Commun. **220**, 137 (2003).
[45]B. Lamprecht, G. Schider, R. T. Lechner, H. Ditlbacher, J. R. Krenn, A. Leitner, and F. R. Aussenegg, Phys. Rev. Lett. **84**, 4721 (2000).
[46]G. B. Smith and V. N. Pustovit, Opt. Commun. **211**, 197 (2002).
[47]F. Claro, Phys. Rev. B **25**, 7875 (1982).
[48]R. Ruppin, Phys. Rev. B **26**, 3440 (1982).